Optimal Fiber Diffusion Model Restoration

Clint Greene*[1], Kate Revill *[2], Cathrin Buetefisch *[2], Ken Rose*[1], and Scott Grafton *[1]

[1] University of California, Santa Barbara
[2] Emory University

Abstract. Assessing the effects of white matter (WM) lesions on structural connectivity as measured by diffusion MRI (dMRI) is invaluable for understanding structure-function relationships. These WM lesions have many etiologies that ultimately lead to attenuation of the anisotropic signature in dMRI signals. Attenuation can produce inaccurate reconstructions of the underlying model of the fiber population. In this paper, we combine methods from image inpainting and estimation theory to develop a novel approach for restoring the fiber model in small to moderate sized WM lesions. Our approach begins by taking healthy reconstructed WM fiber models at the boundary of the lesion and filling in lesioned voxels with their optimal affine estimate moving iteratively in a fast-marching method style until the fiber models in the lesion are restored. We demonstrate with in-vivo simulations on diffusion tensors (DTs) and fiber orientation distributions (FODs) that our approach offers superior performance over multiple restoration approaches. We restore lesioned fiber models in three stroke patients suffering hemiparesis from damaged corticospinal tracts (CST). We show that our method restores diffusivities, anisotropy and orientation of lesioned DTs as well as the amplitudes and orientations of fiber populations in lesioned FODs enhancing tractography and enabling more accurate characterization of lesion connectivity and changes in tissue microstructure in patient populations.

Keywords: image restoration · inpainting · tissue microstructure · disconnection · DTI · HARDI · DSI · FODs · tensors · diffusion MRI · connectomics · spatial normalization · brain lesions

1 Introduction

Diffusion-weighted magnetic resonance imaging (DW-MRI) techniques have been successfully used to non-invasively explore fiber bundle architectures in the brain. These techniques are sensitive to the diffusion of water molecules enabling the characterization of the orientation of bundles of myelinated axons when the water is restricted to diffusion along the long axis of the axons. However, due to pathological injury processes such as gliosis, demyelination, and necrosis, the structural integrity of the axons is compromised, and water is no longer restricted to diffusing along the long axis. These macro and microstructural changes attenuate the anisotropic signature in dMRI signals [1]. Consequently, it remains

challenging to accurately characterize the change in tissue microstructure and the connectivity within lesioned white matter areas which are crucial for studying disconnection syndromes.

Clinical researchers typically measure changes in tissue microstructure by comparing the measurements in the lesion ROI with measurements in healthy tissue from the left-right flipped ROI [2]. Using microstructure measurements from the contralesional side as a model for the original properties is not the most accurate approach because the brain is not symmetric and where it is symmetric, e.g. CST, the tissue measurements are not identical and are less similar to restored tissue measurements. With regards to mapping lesion connectivity, one strategy clinical researchers use is to project the patient's lesion into a normal database of streamlines to approximate the degree of disruption by the lesion to normative [3]. However, this strategy produces a generic estimate of the patients lost connectivity, without any characterization of patient specific disrupted connectivity. Other researchers simply track through the lesioned area to map the lesions connectivity [4]. However, tracking through lesioned areas is known to affect streamline reconstruction and structural networks [5,6].

Another strategy for characterizing lesion connectivity and changes in microstructure is to restore or inpaint the lesioned fiber diffusion model. This has the advantage of more closely preserving the patients native connectivity structure. Prior work has primarily focused on inpainting multiple sclerosis (MS) and tumor lesions in T1 T2 weighted images to improve registration accuracy to a template [7,8]. Recently, a method has been developed to restore fiber orientation distributions (FODs) in MS lesions [9]. They combine diffusion based inpainting and FOD reconstruction in a single step. But they only assessed their performance on an unrealistic simulated lesion of 9 voxels, so it is unclear how it would perform in-vivo. Moreover, its only capable of restoring FODs.

Although a method exists for restoring FODs, a solution that can restore multiple fiber diffusion models, is needed for multiple reasons. The ability to restore diffusion tensors would be beneficial since diffusion tensor imaging (DTI) remains the most popular technique used by clinical researchers for characterizing changes in tissue microstructure and connectivity in lesioned WM tissue. Furthermore, many clinical diffusion datasets in wide use can be reconstructed in myriad ways and contain lesions from the myriad etiologies of WM injury such as white matter hyperintensities in the Rotterdam Study and the Human Connectome Project (HCP) Lifespan study[10,11]. Since there is a great need in clinical research to improve prediction outcomes, the ability of researchers to restore the fiber diffusion models of their choice in a lesion would make such an approach more accessible and have the potential to improve these predictions through improved anatomical delineation of lesion disrupted connectivity and measurement of changes in tissue microstructure.

In this paper, we describe a novel approach that combines methods from diffusion-based image inpainting and estimation theory for restoring fiber diffusion models in WM lesions. Our approach begins by taking healthy WM fiber models at the boundary of the lesion and filling in lesioned voxels with their

optimal affine estimate moving iteratively in a fast-marching method style until the fiber models in the lesion are restored. By leveraging estimation theory, we can minimize the mean squared error (MSE) of fiber models within the lesion, restoring their original shapes and orientations. We demonstrate with realistic in-vivo simulations on diffusion tensors and fiber orientation distributions that our approach offers superior performance over multiple inpainting approaches. Further we restore diffusion tensors and FODs in lesions in three stroke patients suffering hemiparesis and demonstrate that the shape and orientation of the fiber models and the ability to map the lesions connectivity are recovered.

2 Methods

2.1 Diffusion imaging data

The S500 dataset containing 500 subjects was collected from the Washington University-Minnesota Consortium Human Connectome Project [11]. Further analysis was restricted to 210 subjects without familial relation. The diffusion volumes were collected with a spatial resolution $1.25mm^3$, using three shells at b = 1000, 2000, and 3000 s/mm^2 with 90 diffusion directions/shell.

Diffusion volumes were collected for three stroke patients with unilateral motor impairment at Emory University using the HCP Lifespan protocol with a spatial resolution of $1.5mm^3$, using two shells at b = 1500 and 3000 s/mm^2 with 46 diffusion directions per shell and 7 b0s. All datasets were corrected for geometric, eddy current, and motion distortions using the HCP Pipeline scripts.

The diffusion tensors were reconstructed from the diffusion weighted volumes collected with b = 1000 s/mm^2 with weighted least squares in Dipy for the HCP dataset and b = 1500 s/mm^2 for the stroke dataset [13]. Fiber orientation distributions we reconstructed using constrained spherical deconvolution (CSD) in MRtrix with b = 3000 s/mm^2 and $l_{max} = 8$ for both datasets [13,14]. The response function was estimated using the recursive Tax algorithm [15].

2.2 Model estimation

Suppose there is a lesioned fiber diffusion model $\boldsymbol{L}$ lying at the boundary of the lesion and healthy WM tissue. If the model is a diffusion tensor then there are only 6 unique elements of $\boldsymbol{L}$ that need to be estimated i.e. $D_{xx}, D_{yy}, D_{zz}, D_{xy}, D_{xz}, and\ D_{yz}$ because diffusion tensors are positive semi-definite matrices. Similarly, if a more complex spherical deconvolution model is used then at each lesioned voxel the FOD is represented by a real-valued spherical harmonic coefficient vector, F, containing $(l_{max} + 1) \times (l_{max} + 2)$ / 2 elements that need to be estimated. Consider that $\boldsymbol{L}$ has N observed healthy or restored neighboring models, $H_1, H_2, \ldots, H_N \in \mathcal{W}$, the white matter mask. Each unknown element, Y_i e.g. D_{xx} or F_i, is treated as a random variable. The collection of matching neighbor elements forms a random vector $X = [X_1, X_2, \cdots, X_N]$. Then each unknown element Y_i can be estimated from the known neighboring elements of H_i using an optimal affine estimator.

We seek an affine estimator $\hat{Y} = \ a_0 + \sum_{i=1}^{N} a_i X_i$ such that the MSE e.g. $\varepsilon^2 = \ E\left[(Y - \hat{Y})^2\right]$ is minimized. To minimize this expression, we differentiate it with respect to a_i. Differentiating $E\left[(Y - a_0 + \sum_{i=1}^{N} a_i X_i)^2\right]$ with respect to a_0 and setting it to 0 we find that $a_0 = \mu_Y - \sum_{i=1}^{N} a_i \mu_{X_i}$ from which it follows that $\hat{Y} = \ \mu_Y + \sum_{i=1}^{N} a_i \left(X - \mu_{X\,i}\right)$. Letting $\widetilde{Y} = Y - \ \mu_Y$ *and* $\widetilde{X} = X - \ \mu_X$ we can rewrite our MSE criterion as $E\left[(\tilde{Y} - \sum_{i=1}^{N} a_i \tilde{X}_i)^2\right]$.

By differentiating this with respect to the coefficients and setting the result to 0 produces: $E\left[(\tilde{Y} - \sum_{i=1}^{N} a_i \tilde{X}_i)\tilde{X}_j\right] = 0 \quad j = 1, 2, \cdots, N$ which can be rewritten as $E\left[\tilde{X}_j \tilde{Y}\right] = \sum_{i=1}^{N} E\left[a_i \tilde{X}_i \tilde{X}_j\right]$. These sets of equations can be expressed in matrix form as $R_{XY} = (R_{XX})\, a$ where R_{XY} is the cross-correlation vector and R_{XX} is the auto-correlation matrix and a is the coefficient vector. We obtain the optimal coefficients: $a = (R_{XX})^{-1} R_{XY}$.

From this solution it is possible to produce the optimal affine estimate of elements of $\boldsymbol{L}$**:** $L_i = a_1 L_i^{\widetilde{H_1}} + a_2 L_i^{\widetilde{H_2}} + \cdots + a_N L_i^{\widetilde{H_N}} + \ \mu_{Y_i}$, where $\widetilde{H_i} = \ H_i - \mu_{X_i}(1)$ By taking the affine combination of the neighboring healthy elements. Since Y and X are approximately Gaussian, the optimal affine estimate excellently approximates the optimal MMSE estimate of Y. However, to construct an optimal affine estimator at each voxel a distribution of fiber diffusion models must exist at every voxel in the patient.

2.3 Distribution of fiber models

A fiber model distribution at every voxel in the patient can be constructed through spatial normalization. Custom fiber diffusion model templates are constructed using DTI-TK for tensors and FOD Reorientation and ANTs for FODs [16,17,18]. After the templates are constructed, we spatially normalize the patients reconstructed tensors or FODs into its respective custom HCP template using cost-function masking. We then combine the estimated deformation fields to the template for the patients and the HCP subjects to warp a subset of tensor or FOD data from the HCP subjects that corresponds to voxels in the patients lesion and healthy voxels at the boundary.

2.4 Model inpainting

We use a diffusion based inpainting algorithm where the lesion region is filled from its border to the center inspired from [19]. At each iteration, rather than taking a simple average of the known neighboring models, we estimate the unknown model $\boldsymbol{L}$ by taking the affine combination of its healthy neighbors where the coefficients are estimated from the optimal affine estimator in *Eq.*(1). Note that an optimal affine estimator is constructed for each element of the fiber diffusion model for each voxel in the lesion region.

while the lesion region is not empty:
for all $\boldsymbol{L} \in \partial\Omega$:
for all $y \in \boldsymbol{L(y)}$:
$$y = a_1 L_i^{\widetilde{H_1}} + a_2 L_i^{\widetilde{H_2}} + \cdots + a_N L_i^{\widetilde{H_N}} + \mu_{Y_y}$$
$\Omega = \Omega / \partial\Omega$
where $\widetilde{H_i} = H_i - \mu_{X_y} \in \bar{\Omega} \cap \mathcal{W}$ *and* $y \in [L_1, L_2, \cdots, L_N]$, $\boldsymbol{L}$ is the model to inpaint, Ω is the lesion region, $\bar{\Omega}$ its complement (the voxels outside Ω), $\partial\Omega$ its border (voxels of Ω having one of its 6 cube neighbors in $\bar{\Omega}$).

3 Results

3.1 Simulation in-vivo

We demonstrate the efficacy of our approach by simulating a lesion within a healthy HCP subject that is not part of the model distribution. The lesion was created by adding Rician noise to a cuboidal region consisting of 1035 voxels (129 cm^3) until the SNR = 3. The lesioned voxels are then inpainted with a baseline approach and our optimal approach. For our baseline, we use the same diffusion based inpainting algorithm as used in the optimal estimation where the inpainted model is estimated by simply taking an average of its neighbors [19]. The results of inpainting the tensors (top) and FODs (bottom) with both approaches is shown in Figure 1 within the transparent border.

Column C shows the ground truth reconstructed tensors (top) and FODs (bottom). The baseline approach is shown in column B and our optimal approach is show in column D. At first glance, the baseline approach appears to provide a reasonable restoration of the tensors but upon closer inspection many tensors have different anisotropy (shape) and orientation (color) relative to the ground truth tensors. For FODs restored using the baseline approach it is immediately clear that they differ in both magnitude and orientation with respect to the ground truth. Our optimal approach more accurately preserves the anisotropy and orientation of the ground truth tensors and the magnitude and orientation of the ground truth FODs.

The mean angular error (MAE) is plotted for the primary fiber direction for tensors on the left and on the right for FODs (solid) from the HCP template mean normalized into the lesion area (green), restored using the baseline approach (orange), and restored using our optimal approach (blue) with respect to the primary fiber direction from the respective ground truth tensors and FODs for lesion sizes varying from 6 voxels to 1035 voxels in Figure 2. For the smallest lesions, the difference in MAE is negligible for all the approaches and the FODs MAE is less than the tensors MAE. However, as lesion size increases the FODs MAE quickly outpaces the tensors MAE. In general, the template average has the largest MAE while our optimal approach has the smallest as lesion size increase. The MAE for the baseline approach grows more rapidly than our optimal approach for both tensors and FODs and for large lesions the MAE is twice as large compared to our optimal approach. On the right in Figure 2, the MAE for

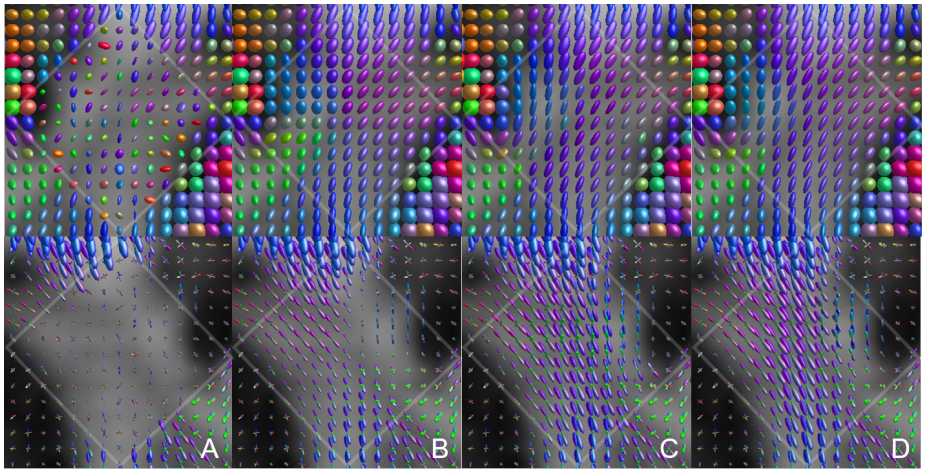

Fig. 1. In-vivo simulated model restoration: The lesion region is demarcated by the transparent border. Rician noise is added to the original diffusion signal until SNR = 3 producing the tensors (top) and FODs (bottom) in A. The baseline approach in B appears to provide reasonable approximation of normal tensors but upon closer inspection the restored tensors differ in anisotropy and orientation, while for FODs there are large deviations in magnitude and orientation from the ground truth The ground truth reconstructions are in C. Tensors and FODs restored using our optimal approach are in D. Notice that the tensors and FODs restored using our approach more closely match the ground truth in terms of orientation and shape compared to the baseline.

the second fiber population is plotted as the dotted line and is typically twice as large as the MAE for the primary FOD fiber population. The trends for the angular error in the second fiber population mirror those seen in the primary FOD fiber population. Our optimal approach achieves the smallest MAE.

On the top left of Figure 3, the root mean squared error (RMSE) in fractional anisotropy (FA) with respect to the ground truth is measured for varying lesion sizes. The RMSE starts high and then slowly decreases until its constant with increasing lesion size for the template mean (green). The RMSE of FA values extracted from the flipped ROI in the contralesional area (red) with respect to the original FA values also starts high and then grows slowly with increasing lesion size. For lesion sizes < 200 voxels, the baseline and optimal approach have almost identical trends, but for larger sizes the baseline error grows much faster than for our optimal approach. At large lesion sizes the baseline approach again has an error almost double our optimal approach. For axial diffusivity (AD) on the top right, the template mean and optimal AD RMSEs both grow moderately with increasing lesion size while the RMSE for the baseline and flipped case grow faster. On the bottom row in Figure 3, the RMSEs for mean diffusivity (MD) and radial diffusivity (RD) are plotted. The MD and RD RMSE for the flipped case grows the fastest with increasing lesion size while the template mean, the

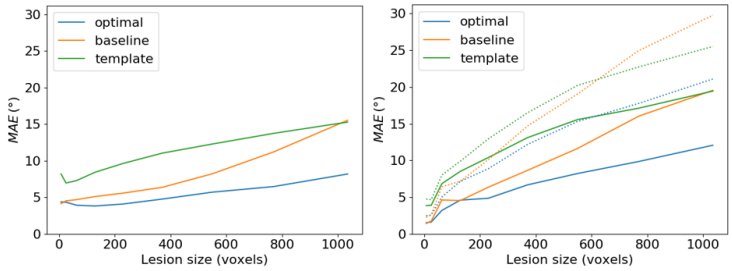

Fig. 2. Analysis of angular error: The MAE is plotted on the left for tensors and on the right for FODs (solid) for the primary fiber direction for varying lesions sizes. The MAE for the smallest lesion sizes is comparable across all approaches and the FODs MAE is smaller than the tensors MAE. However, the FODs MAE quickly outpaces the tensors MAE at larger lesion sizes. The template average (green) has the largest MAE while our optimal approach (blue) as the smallest as lesion size increase. The MAE for the baseline approach (orange) grows more rapidly than our optimal approach for both tensors and FODs. Typically, the baseline approach has a MAE twice as large as of our optimal approach. On the right, the MAE for the second fiber population is plotted as the dotted line. It is typically twice as large as the MAE for primary FOD fiber population. The MAE trend in the secondary fiber population mirrors those seen in the primary FOD fiber population for all restoration approaches. Our optimal approach minimizes the MAE the most compared to the baseline and template approaches.

baseline, and optimal approachs RMSE grow slowly. Interestingly, there is not much gain in terms of RMSE for MD and RD between the baseline and our optimal approach. In general, our optimal approach has the smallest RMSE and grows the slowest with increasing lesion size while the baseline outperforms the template mean which outperforms the flipped-case for all tissue measures.

3.2 Lesion restoration

The restoration results using our optimal approach are plotted in Figure 4 for three patients. The lesion region for each patient that undergoes restoration is demarcated in red on the coronal FA slice in column A. The lesioned tensors before and after the restoration are seen in columns B and C in Figure 4. In column B, the tensors in the lesion area have lost their normal color (orientation) and shape (anisotropy). Notice that the restored tensors in column C have both normal appearing shape and color. The lesioned FODs before and after restoration are plotted in columns D and E. In column D, the lesioned FODs have lost their normal orientation and magnitude. The orientation and magnitude of FODs in the lesion are recovered after undergoing restoration using our optimal approach. Moreover, the restored tensors and FODs demonstrate high spatial coherence with the surrounding healthy white matter tensors and FODs.

The restoration of scalar tissue microstructure measures AD, MD, and RD are plotted in Figure 5 for patient 1 on the same coronal plane. In the top row are

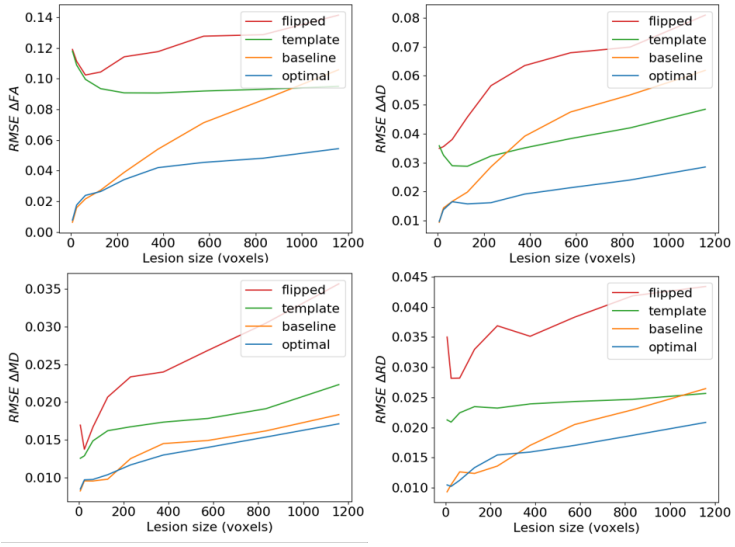

Fig. 3. RMSE of tissue microstructure measurements: On the top left, RMSE FA for the baseline (orange) and our optimal approach (blue) show nearly identical trends for lesion sizes < 200 voxels. The baseline RMSE FA increases more rapidly compared to our optimal approach and is nearly twice as large at larger lesion sizes. For the template mean (green) the RMSE gradually decreases until becoming constant as the lesion size increases. The RMSE of FA values extracted from the flipped ROI in the contralesional area (red) with respect to the original FA values grows slowly with increasing lesion size. On the top right the RMSE for axial diffusivity (AD) is plotted. The template mean and optimal AD RMSEs both grow moderately with increasing lesion size while the RMSE for the baseline and flipped case grow faster. On the bottom row, the RMSEs for mean diffusivity (MD) and radial diffusivity (RD) are plotted. The MD and RD RMSE for the flipped case grows the fastest with increasing lesion size while the template mean, the baseline, and optimal approachs RMSE grow slowly. For MD and RD there is not much gain with our optimal approach over the baseline. In general, our optimal approach has the smallest RMSE and grows the slowest with increasing lesion size for all tissue measures.

the measures before the restoration and in the bottom row after the restoration. The lesion area is demarcated in red. Notice that after restoration using our optimal approach that the lesion area has been restored to a normal appearance for all the scalar diffusivities.

To demonstrate the improved mapping of lesion connectivity after fiber model restoration, we perform deterministic tractography before and after restoration on FODs in MRtrix with default settings using the SD_STREAM algorithm from a seed image consisting of two voxels below the lesion area with 1000 seeds per voxel [14]. In Figure 6, the tractography results before the restoration (top) and after the restoration (middle) are displayed on top of the magnified portion of their lesion in the sagittal FA slice which is denoted by the arrow (bottom).

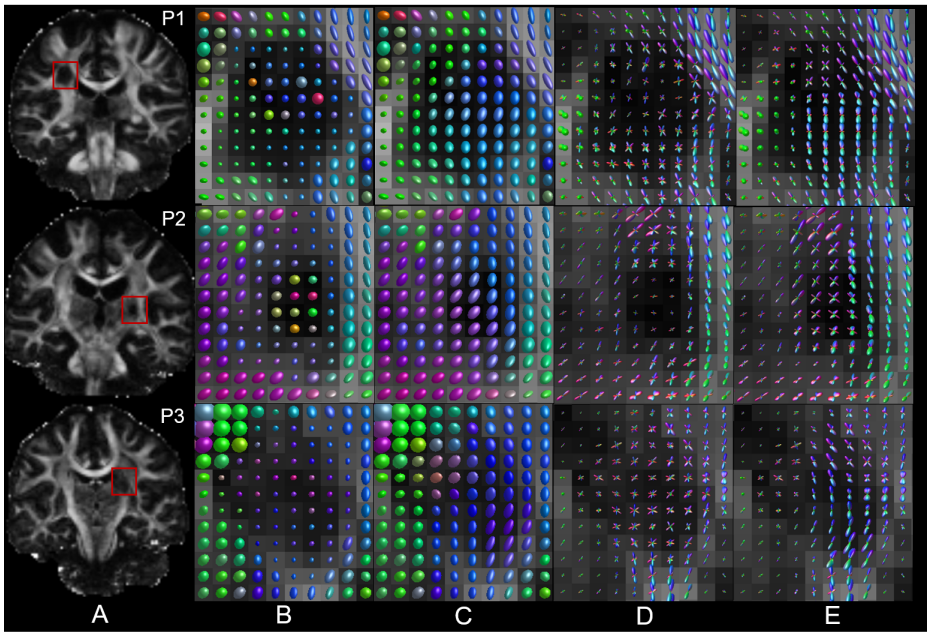

Fig. 4. Restoration results for three stroke patients: The lesion regions where models undergo restoration is demarcated in red in column A. The average lesion size is 390 voxels. In column B are the tensors before the restoration and afterwards in column C. The loss of anisotropy (shape) and proper orientation (color) of healthy white matter tissue in the CST are visible in column B. In column C, our approach restores the orientations and anisotropy of the tensors to a normal appearance. Similarly, the FODs in the lesion area of column D have lost their normal orientation and magnitude. After underoing restoration using our optimal approach the normal orientation and magnitude of the FODs in the lesion area have been recovered in E. The restored tensors (C) and FODs (E) demonstrate high spatial coherence with their surroundings.

In all three patients, once the tracking enters portions of the lesion area it prematurely terminates before the restoration, preventing an accurate mapping of connectivity within the lesion. After the FODs have been restored, tracking through the lesion area becomes feasible enabling a more accurate mapping of the lesions connectivity.

4 Discussion

Using in-vivo simulations and stroke patient data, we demonstrated the ability of our novel approach for accurately restoring both the orientation and magnitude of FODs and the orientation, anisotropy, and tissue microstructure measures of diffusion tensors in WM lesions. Our optimal affine estimator approach offers superior performance over a diffusion based inpainting approach

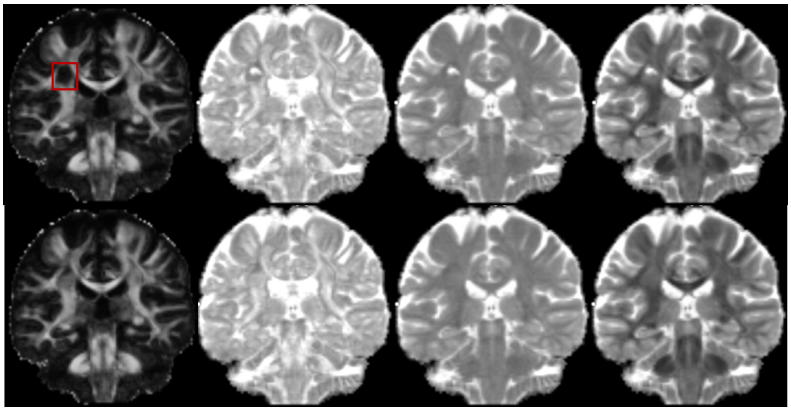

Fig. 5. Coronal view of tissue microstructure measures before (top) and after (bottom) restoration for patient 1: From left to right axial diffusivity, mean diffusivity, and radial diffusivity. The lesion area is demarcated in red. The lesion area has been restored to a normal appearance for all measures.

that takes the average of neighboring tensors for inpainting a lesioned area as well as the trivial copy and pasting of tensors or FODs from the normalized HCP tensor or FOD template.

Simple neighbor averaging performs well for very small lesions. However, as the lesion sizes increases, it introduces increased blurring that compounds moving inward. The increased blurring is reflected by the large increases in angular error and error in scalar measures such as FA or AD as the lesion sizes increase. Our optimal approach performs well at restoring tensors and FODs across all lesion sizes with only modest increases in angular error and error in scalar measures as the lesion size increases because as the algorithm moves inward, the fiber diffusion models are inpainted with their optimal affine combination of their neighbors such that the MSE is minimized. Consequently, blurring is reduced as the algorithm moves toward the center of the lesion.

Although performance was only measured on simulated cuboidal lesions, our method is applicable to lesions of any shape. Besides lesion size and location, the quality of the restoration depends on the initial healthy fiber diffusion models that are optimally combined to inpaint the first set of models in the lesion area. If the healthy models are corrupted by noise or by proximity to the lesion, it will get propagated into all subsequent inpainted models. Consequently, we recommend overestimating the lesion mask and carefully defining the white matter mask to ensure all models used in the initial stages are in fact healthy. Moreover, despite only demonstrating the restoration of lesioned diffusion tensors and FODs, orientation distribution functions (ODFs) from QBI could also be restored using our approach by representing them with an orthonormal spherical harmonic basis and using FOD reorientation to build a distribution of ODFs.

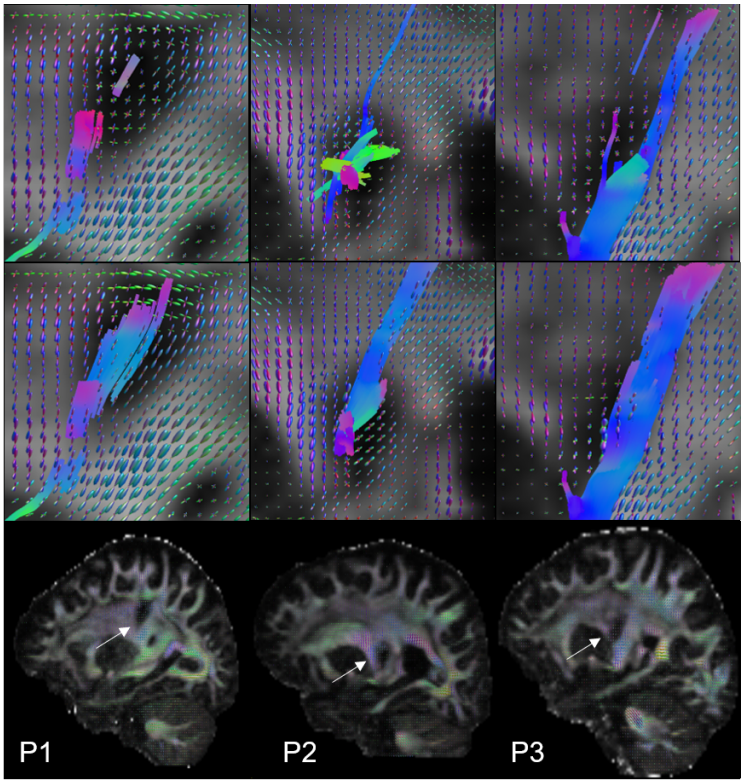

Fig. 6. Deterministic tractography results before (top) and after (middle) restoration: Before the restoration, a portion of all three patients streamlines prematurely terminate once they enter the lesion area, making it difficult to study the patients lesion connectivity. After the restoration, tractography can be performed more accurately because the FODs have been restored, enhancing the tracking and mapping of connectivity in the lesion areas. The results are plotted on top of magnified portion of the lesion area in the sagittal FA slice (bottom).

Clinicians and researchers could find our approach beneficial for restoring fiber diffusion models in lesioned areas in their clinical diffusion datasets because it not only improves the accuracy of measuring changes in tissue microstructure relative to measurements from the contralesional area but also improves the accuracy of tractography results and the mapping of connectivity from the lesion for improved study of structure-function relationships and outcome prediction. To apply our approach, visit https://github.com/clintg6/OFDMR.

References

1. Chiang, Chia-Wen, et al. "Quantifying white matter tract diffusion parameters in the presence of increased extra-fiber cellularity and vasogenic edema." Neuroimage

101 (2014): 310-319.
2. Song, Jie, et al. "DTI measures track and predict motor function outcomes in stroke rehabilitation utilizing BCI technology." Frontiers in human neuroscience 9 (2015): 195.
3. Greene, Clint, Matt Cieslak, and Scott T. Grafton. "Effect of different spatial normalization approaches on tractography and structural brain networks." Network Neuroscience 2.3 (2018): 362-380.
4. Langen, Carolyn D., et al. "Disconnection due to white matter hyperintensities is associated with lower cognitive scores." Neuroimage 183 (2018): 745-756.
5. Theaud, Guillaume, et al. "Impact of white-matter hyperintensities on tractography." 25th Annual Meeting of the International Society for Magnetic Resonance in Medicine (ISMRM). Honolulu: International Society for Magnetic Resonance in Medicine. 2017.
6. Greene, C., Cieslak, M., Grafton, S. T. (2018). Effect of different spatial normalization approaches on tractography and structural brain networks. Network Neuroscience, 2(3), 362-380.
7. Sdika, Michal, and Daniel Pelletier. "Nonrigid registration of multiple sclerosis brain images using lesion inpainting for morphometry or lesion mapping." Human brain mapping 30.4 (2009): 1060-1067.
8. Prados, Ferran, et al. "Fully Automated Patch-Based Image Restoration: Application to Pathology Inpainting." International Workshop on Brainlesion: Glioma, Multiple Sclerosis, Stroke and Traumatic Brain Injuries. Springer, Cham, 2016.
9. Sun, Wei, Lilyana Amezcua, and Yonggang Shi. "FOD restoration for enhanced mapping of white matter lesion connectivity." International Conference on Medical Image Computing and Computer-Assisted Intervention. Springer, Cham, 2017.
10. Hofman, Albert, et al. "The Rotterdam Study: 2016 objectives and design update." European journal of epidemiology 30.8 (2015): 661-708.
11. Glasser, Matthew F., et al. "The minimal preprocessing pipelines for the Human Connectome Project." Neuroimage 80 (2013): 105-124.
12. Garyfallidis, Eleftherios, et al. "Dipy, a library for the analysis of diffusion MRI data." Frontiers in neuroinformatics 8 (2014): 8.
13. Tournier, J-Donald, Fernando Calamante, and Alan Connelly. "Robust determination of the fibre orientation distribution in diffusion MRI: non-negativity constrained super-resolved spherical deconvolution." Neuroimage 35.4 (2007): 1459-1472.
14. Tournier, JDonald, Fernando Calamante, and Alan Connelly. "MRtrix: diffusion tractography in crossing fiber regions." International journal of imaging systems and technology 22.1 (2012): 53-66.
15. Tax, Chantal MW, et al. "Recursive calibration of the fiber response function for spherical deconvolution of diffusion MRI data." Neuroimage 86 (2014): 67-80.
16. Raffelt, David, et al. "Reorientation of fiber orientation distributions using apodized point spread functions." Magnetic Resonance in Medicine 67.3 (2012): 844-855.
17. Zhang, Hui, et al. "Unbiased white matter atlas construction using diffusion tensor images." International conference on medical image computing and computer-assisted intervention. Springer, Berlin, Heidelberg, 2007.
18. Avants, Brian B., et al. "Symmetric diffeomorphic image registration with cross-correlation: evaluating automated labeling of elderly and neurodegenerative brain." Medical image analysis 12.1 (2008): 26-41.
19. Telea, Alexandru. "An image inpainting technique based on the fast marching method." Journal of graphics tools 9.1 (2004): 23-34.